Boundary Layer Studies on the Phoenix Sailplane

By AUGUST RASPET and DEZSÖ GYÖRGYFALVY, Aerophysics Department, Mississippi State University

Presented at the 8th OSTIV Congress, Cologne, Germany, June, 1960

Introduction

Since the first application of laminar airfoils to sailplanes was made on the RJ-5 sailplane, considerable technology has been developed which permits the ultimate to be attained from these airfoils. In particular, the importance of wave-free contours was found to be of utmost importance by the series of profile drag measurements made in flight on the RJ-5 [1].

However, no essential advance in the design of laminar airfoils was made until Eppler[2] made his contribution to airfoil design. Since the first practical test of these new airfoils was made on the sailplane, Phoenix [3], it was felt by the authors that a critical examination of the Phoenix would provide much useful information and would contribute to further improvements of Eppler's method for designing airfoils.

The Phoenix lent itself admirably to the flight examination of these new laminar airfoils in that the sailplane was constructed of Fiberglas-plastic sandwich, which had sufficient geometric stability to ensure that the airfoils produced on the ground would be retained in the air under normal flight loads.

That these airfoils contributed considerably to the high performance of the Phoenix has already been reported [4]. With an aspect ratio less than 18, the Phoenix attains a maximum glide ratio of 40.

In view of the excellent geometric stability of the sandwich construction on the Phoenix and the unique mathematical approach to the airfoil design for this sailplane, a concentrated flight research aimed at examining the boundary layer development on the Phoenix airfoil was conducted at Mississippi State University during the spring of 1959. It is the purpose of this paper to report on the research conducted on the Phoenix airfoil. In general, the airfoil was found to fulfill the design conditions laid down by Eppler. In one particular, it even exceeded all expectations in that it attained a maximum lift coefficient of 1.75, considerably higher than classical laminar airfoils.

Description of Flight Research

In order to insure that the measurements made during the flight research on the Phoenix would be truly representative of the airfoil as computed by Eppler, the entire upper surface of the Phoenix wing was smoothed to a waviness accuracy of 0,05 mm., measured with a wave gauge having its outside contact points spaced at 5 cm. The bottom of the wing was contoured to an accuracy of 0,05 mm only in the test section, about one meter in extent.

The test area was placed at the theoretical mean aerodynamic chord, as shown in Figure 1. It will be noted that the measurements of profile drag were made along three chordwise lines spaced at 0,15 m. This was done to eliminate the effect of such small geometric spanwise variations as might exist in the airfoil from that of the EC86 (-3) -914. Even so, no measurement of the absolute values of the coordinates of the airfoil on the Phoenix was made; however, since the final assembly was made in the original molds, one can assume that the accuracy was at least as good as the molds.

Profile drag measurements were made using an integrating wake rake designed according to the stipulations of Silverstein and Katzoff [5]. Differential pressures were measured using sensitive diaphragm type airspeed indicators. The measuring system, consisting of integrating wake rake, Kiel total pressure tube, airspeed indicator and tubing, was dynamically balanced so that the rate of change of static pressure would not be reflected in the differential pressure readings.

Boundary layer profile measurements were made with a rake consisting of nine stainless steel tubes 1,0 mm in outside diameter, with flattened inlet of 0,2 mm in height. The total pressure tubes were located at heights above the surface as follows: 0,20, 0,30, 0,53, 0,81, 1,37, 1,90, 3,94, 6,60, 14,20 millimeters. The one static pressure tube was located 5,0 mm from the surface.

Pressure distribution measurements were obtained by a twenty-tube plastic belt, having properly spaced orifices, which was taped to the airfoil [6].

Fig. 1

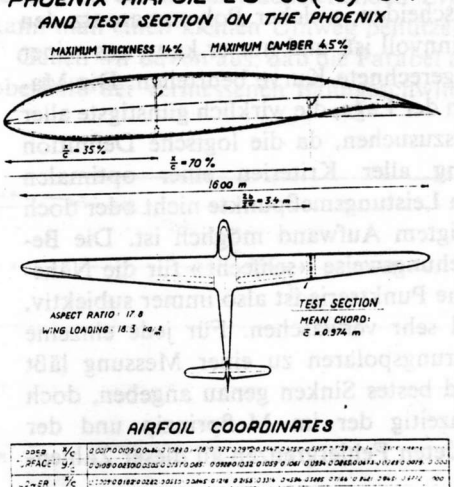

Fig. 2

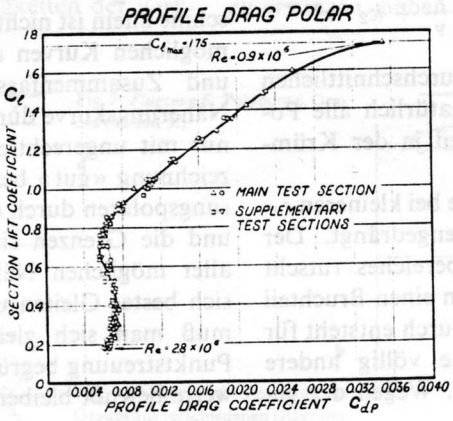

Fig. 3

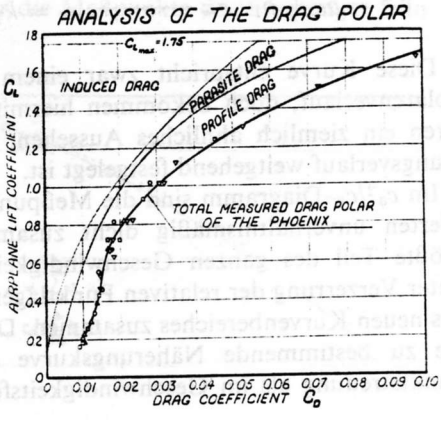

BOUNDARY LAYER PROFILES ON UPPER SURFACE

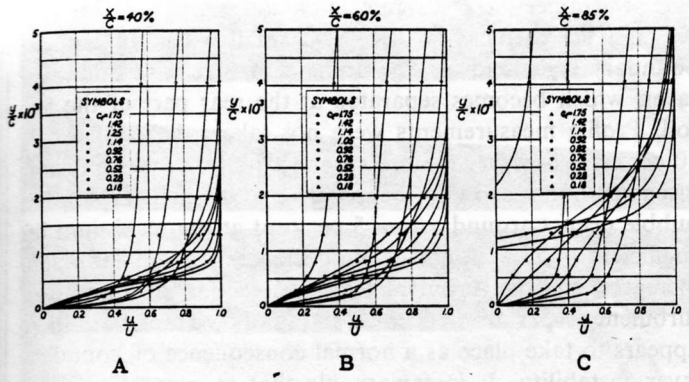

Fig. 4

BOUNDARY LAYER PROFILES ON LOWER SURFACE

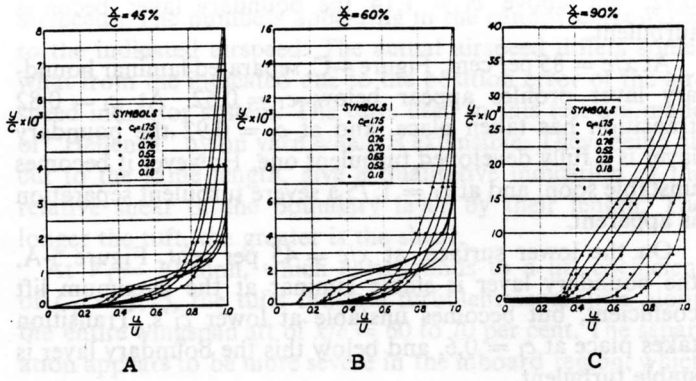

Fig. 5

A photo manometer consisting of twenty water filled u-tubes was used to record the boundary layer profiles and the pressure readings from the plastic belt.

Tuft photos were taken to confirm the location of turbulent boundary layer separation.

Profile Drag Measurements

In Figure 2 are shown the actual profile drag measurements at various section lift coefficients. It will be noted that these readings were made in the range of Reynolds number, Re = 0,9 to 2,85 million. By the very nature of flight research, it is not possible on one vehicle to make measurements at a constant Reynolds number. However, the measurement shown in Figure 2, displays exactly how the profile drag varies on an aircraft of constant wing loading. Therefore, such a display, while not as clearly correlated with theory, does illustrate actual flight conditions.

It will be seen in Figure 2 that there is a very small systematic deviation of the main test section results from those taken on either side. The profile drag polar clearly shows two low drag regions predicted by Eppler. At $c_l = 0{,}175$, the lowest lift coefficient tested, the profile drag amounts to $c_{dp} = 0{,}006$. As the lift coefficient increases the profile drag grows to $c_{dp} = 0{,}007$ and remains nearly constant between $c_l = 0{,}3$ and 0,5. Above $c_l = 0{,}5$ the drag decreases again and reaches its minimum value of $c_{dp\ min} = 0{,}0056$ at $c_l = 0{,}7$. The test data show, however, evidence that the so-called low drag "bucket" might be less pronounced under certain conditions. Above $c_l = 0{,}8$ the drag begins to rise rapidly due to turbulent separation advancing forward from the trailing edge on the upper surface of the airfoil. The stall, however, does not occur immediately and the maximum section lift coefficient is seen to be as high as $c_{l\ max} = 1{,}75$. Interestingly, the maximum section lift coefficient determined by integration of the pressure distribution agrees exactly with the airplane maximum lift coefficient computed from the stalling speed and the wing loading. These two independent measurements clearly validate the high lift coefficient attainable by the Phoenix airfoil.

In order to illustrate the importance of the profile drag as a component of the total drag, a breakdown of the Phoenix drag polar is presented in Figure 3. It was assumed that the measured profile drag polar, which is strictly valid only for one given section, would approximate the resultant profile drag polar, since the test section was at the main aerodynamic chord. Thus, when the profile drag shown in Figure 2 is subtracted from the measured total drag the remaining part should consist of the induced and parasite drag. The induced drag is calculated by the well known formula:

$$C_{Di} = \frac{C_L^2}{\pi\lambda}(1 + \delta)$$

where the induced drag increment, δ, is assumed to be 3,5 per cent, in accordance with the aspect ratio, 17,8, taper ratio, 2,6, and zero washout of the Phoenix wing. Thus, the remaining portion is considered as parasite drag.

The relative values of the drag components are shown below in per cent of the total drag:

Lift coefficient	1.75	1.40	1.00	0.70	0.40	0.175
Induced drag %	53	59	61	51	21	6
Profile drag %	26	32	32	31	52	62
Parasite drag %	21	9	7	18	27	32

Boundary Layer Development

Boundary layer profiles were recorded throughout the entire speed range at the chordwise stations x/c = 10, 20, 30, 40, 50, 60, 70, 75, 80, and 85 per cent on the upper surface and x/c = 10, 20, 30, 45, 60, 70, and 90 per cent on the lower surface. Selections of the boundary layer profile measurements are shown in Figures 4 and 5 for three representative chordwise positions of both upper and lower surfaces. The profiles are given consistently for the same lift coefficients, c_l = 1,75, 1,42, 1,14, 0,92, 0,76, 0,52, 0,28, and 0,18, which correspond to the following indicated airspeeds[1]: V_I = 30, 35, 40, 45, 50, 60, 80, and 100 mph. In some cases additional profiles are also indicated to show more clearly the transition process.

On the upper surface at x/c = 40 per cent, Figure 4-A, the profiles are seen to be laminar for all lift coefficients below $c_l = 1{,}00$. At $c_l = 0{,}28$ the profile become slightly inflected, indicating a tendency of the laminar boundary layer toward instability. At $c_l = 1{,}14$, a transition profile occurs, and at $c_l \geqq 1{,}25$, a fully developed turbulent boundary layer exists. At x/c = 60 per cent, Figure 4-B, inflected laminar boundary layer profiles occur at $c_l \leqq 0{,}52$. A stable laminar boundary layer is present between $c_l = 0{,}76$ and

[1] Indicated airspeed differs from that of calibrated one by the position and instrument reading error of the airspeed indicator system

0,92, but above $c_l = 1{,}14$ the boundary layer becomes turbulent.

At $x/c = 85$ per cent, Figure 4-C, separated laminar boundary layer profiles appear below $c_l = 0{,}52$. At $c_l = 0{,}82$ transition has taken place, and at $c_l = 0{,}92$ the boundary layer is a fully developed turbulent one. However it becomes unstable soon, and at $c_l = 1{,}75$ a severe turbulent separation is apparent.

On the lower surface, at $x/c = 45$ per cent, Figure 5-A, the boundary layer is stable laminar at the maximum lift coefficient, but becomes unstable at lower c_l's. Transition takes place at $c_l = 0{,}6$, and below this the boundary layer is stable turbulent.

At $x/c = 60$ per cent, Figure 5-B, the profile at $c_l = 1{,}75$ is still laminar but already inflected. With decreasing lift coefficient the flow becomes more and more unstable until at $c_l = 0{,}76$, transition begins and below $c_l = 0{,}70$, a fully developed turbulent boundary layer exists.

At $x/c = 90$ per cent, Figure 5-C, the boundary layer is turbulent throughout the entire flight regime. At low lift coefficients the turbulent boundary layer becomes considerably thickened and unstable. Below $c_l = 0{,}52$, a thin separated layer is apparent near the surface.

The results of the boundary layer measurements are shown in a graphic display in Figure 6. The character of the boundary layer is indicated by proper symbols at each individual test station for various values of section lift coefficient. Symbols of the same gender delineate the extent of the different types of boundary layer flow along the chord.

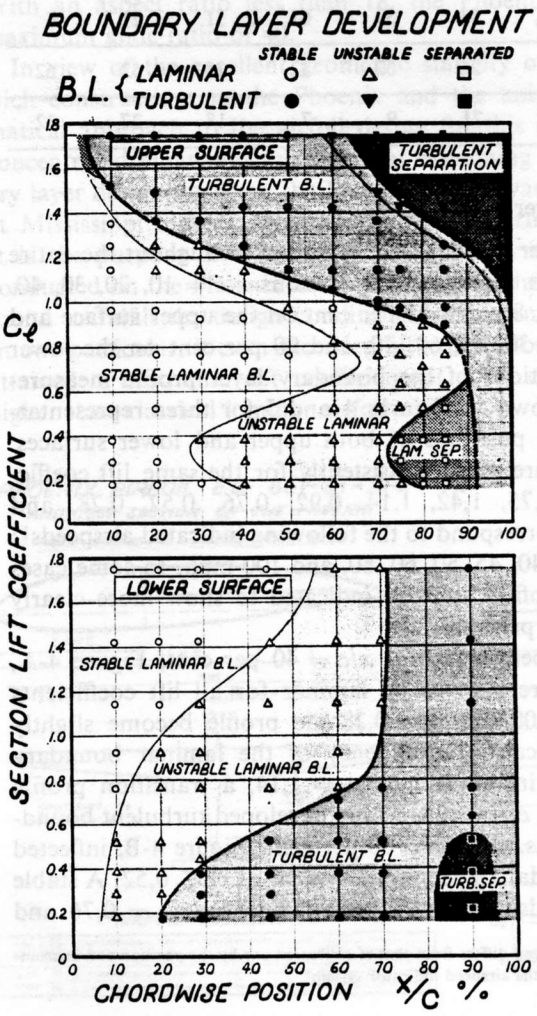

Fig. 6

On the upper surface, significant features are the following: At high lift coefficients there is a small extent of laminar boundary layer and a large domain of turbulent boundary layer, which becomes separated at the rear part of the airfoil. Profile measurements were not taken ahead of $x/c =$ 10 per cent, however the pressure distribution measurements discussed later show evidence that a laminar separation bubble occurs around x/c — 5 per cent at the maximum lift coefficient. As the lift coefficient decreases the laminar extent increases, and the turbulent region as well as the amount of turbulent separation decreases rapidly. Transition here appears to take place as a normal consequence of boundary layer instability. It is remarkable that at $c_l = 0{,}7$ (corresponding to L/D max), the laminar boundary layer extends back to $x/c = 90$ per cent, and instability begins only after $x/c = 65$ per cent. Below $c_l = 0{,}65$ the limit of the laminar instability moves rapidly forward, and laminar separation occurs at $x/c = 70$ to 80 per cent. It is peculiar that in the vicinity of $c_l = 0{,}3$ the instability begins as far forward as $x/c = 30$ per cent, but the consequent laminar separation does not occur until $x/c = 70$ per cent. At very low lift coefficients both the instability and separation take place somewhat further back than the above values.

Since boundary layer measurements were not taken behind $x/c = 85$ per cent, an extrapolation of the data was necessary for the region near the trailing edge. In the case of turbulent separation a study of the tuft photographs, Figure 7. helped to determine the existing conditions. Accordingly. the separation begins at about $c_l = 1{,}0$. At lower lift coefficients, where laminar separation occurs, the transition and re-attachement of the boundary layer was predicted according to Owen's criterion [7], which states that a short bubble occurs whenever

$$Re\delta^*_{sep} = \frac{U_{sep}\,\delta^*_{sep}}{\nu} \geqq 450$$

that is, when the Reynolds number of the boundary layer at separation, based on the displacement thickness, exceeds a critical limit of about 450. In the present case the Reynolds numbers in question are of the order of 1800, which indicates the occurrence of a short bubble. The length of a short bubble is about 100 times the displacement thickness at separation. In the case of the Phoenix airfoil, this implies a bubble length of 6 to 12 per cent of the chord. Consequently, it can be supposed that the separated laminar boundary layer becomes turbulent and shortly after re-attaches somewhere in the vicinity of $x/c = 90$ per cent.

On the lower surface there is a large domain of laminar boundary layer at high lift coefficients, which extends as far back as $x/c = 72$ per cent. The position of the transition remains nearly the same until $c_l = 1{,}0$, but the limit of the instability moves forward to $x/c = 20$ per cent. Below $c_l =$ 1,0, the extent of the turbulent boundary layer rapidly increases and at $c_l = 0{,}2$ transition takes place already at $x/c = 20$ per cent. There is a wide area of unstable laminar boundary layer between lift coefficients, $c_l = 0{,}7$ and 1,3. This implies low shear and consequently low skin friction drag in that regime. It seems to be desirable to extend this low shear area over a larger portion of the airfoil, particularly for the regime of low lift coefficients. There are evidences of turbulent separation at $x/c = 90$ per cent and below $C_L = 0{,}52$. However, the exact boundaries of the separated region were not detected.

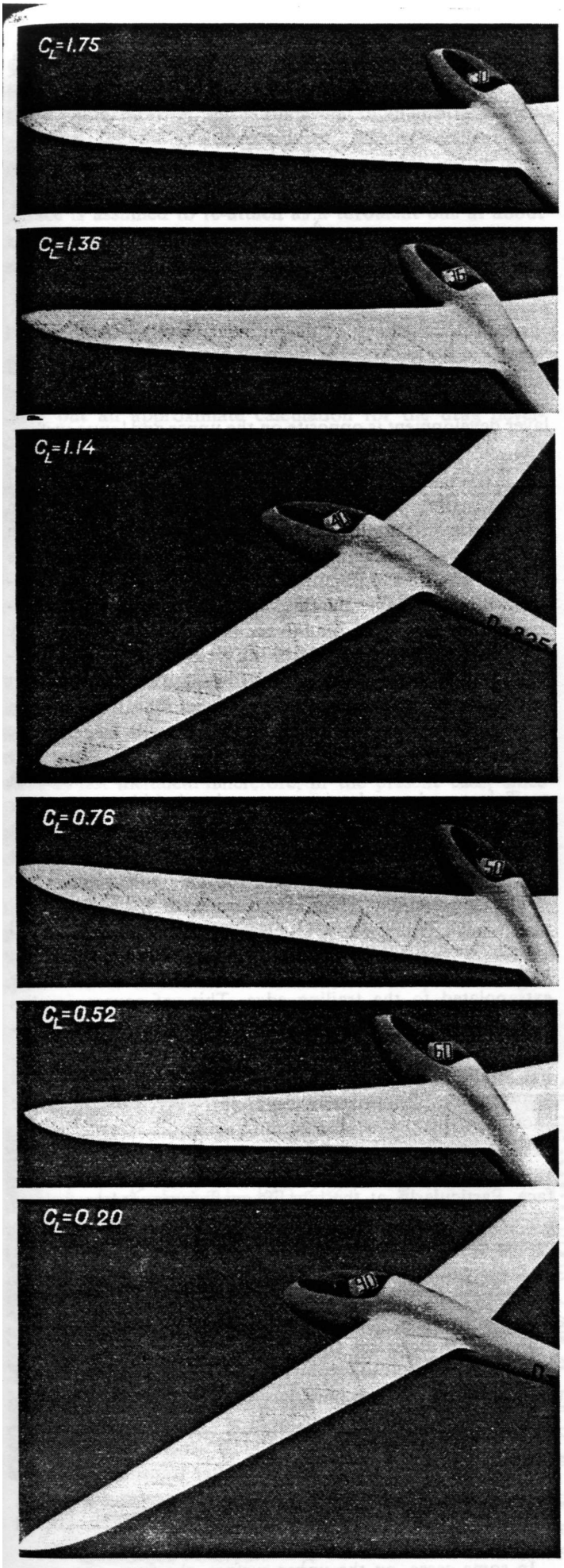

Fig. 7

Figure 7 shows tuft photographs taken in flight at several airspeeds. The numbers appearing in the canopy correspond to the indicated airspeed. The actual airspeed differs somewhat from the indicated due to the position error of the airspeed indicator system. The tufts used in this test are made of "Hellenca" nylon yarn which is extensible. They, being all cut to the same length, give a qualitative indication of the relative shear of the boundary layer by their length. The longer the tuft, the greater is the shear.

At $V_i = 30$ mph, which corresponds to a lift coefficient of $C_L = 1{,}75$, the tufts indicate turbulent separation along the entire wingspan aft of $x/c = 60$ to 70 per cent. The separation appears to be more severe in the inboard region, which behavior assures good lateral stability in the stall. The tufts in the separated region indicate flow towards the root. This is caused by a vortex being shed at the wing root juncture.

The photograph taken at $V_i = 36$ mph, $C_L = 1{,}36$, indicates that the beginning of the separation has moved back to about $x/c = 80$ per cent.

At $V_i = 40$ mph, $C_L = 1{,}14$, the separated area on the wing is reduced to a narrow strip along the trailing edge, nevertheless intensive separation is still present at the wing root juncture, and it persists until $C_L = 0{,}47$. Below this lift coefficient the tufts show completely attached flow. The reason for the separation at the wing root lies in the fact that the boundary layer has built up on the side of the fuselage and is already fairly thick when it enters the wing fuselage intersection.

It should be noted that laminar separation which occurs at low lift coefficients cannot be detected by tufts, since the separated layer is thinner than the tufts.

Pressure Distribution Measurements

Figure 8 shows the pressure distributions around the Phoenix airfoil given in non-dimensional form.

$$\left(\frac{U}{V}\right)^2 = 1 - c_p = 1 - \frac{p - p_o}{q_o}$$

where U/V is the velocity ratio, c_p is the pressure coefficient, p and p_o are the local and free stream static pressures and q_o is the free stream dynamic pressure.

For the sake of easier survey, the curves for the upper and lower surfaces are displayed separately. Also, the curves for the lower surface are presented in a magnified scale. The position of the transition and laminar separation are marked by arrows pointing to the proper points of the curves.

On the upper surface, a noteworthy feature of the curve at $c_l = 1{,}75$ is the "plateau" of constant pressure between $x/c = 3$ and 5 per cent, which is the usual symptom of a laminar separation bubble. The nearly constant pressure region of the same curve behind $x/c = 70$ per cent is a result of the turbulent separation. At lower lift coefficients, the above plateau does not appear, showing that transition takes place here as a normal consequence of laminar boundary layer instability. At lift coefficients between $c_l = 1{,}14$ and 0,76 the minimum pressure occurs at $x/c = 11$ to 16 per cent, nevertheless a remarkably large extent of laminar boundary layer exists after the pressure peak in spite of the adverse pressure gradient. Moreover, at $c_l = 0{,}76$ the laminar boundary layer remains stable as far back as $x/c = 65$ per cent. It is also interesting that at low lift coefficients the laminar

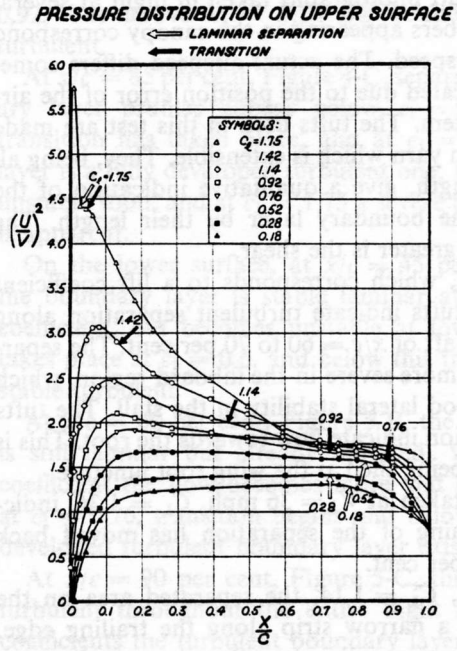

Fig. 8a

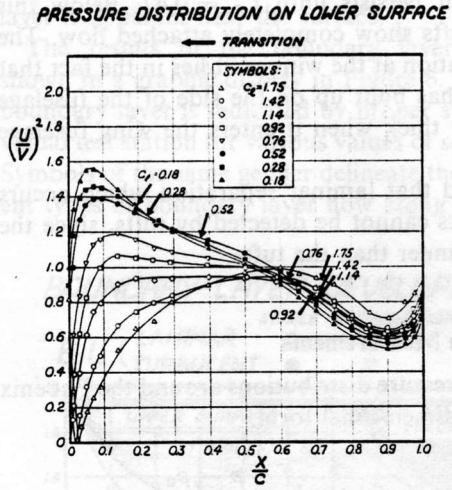

Fig. 8b

boundary layer becomes unstable relatively soon, although the pressure gradient is favorable to $x/c = 75$ per cent. Here laminar separation takes place at or soon after the minimum pressure point.

On the lower surface of the airfoil, at lift coefficients, $c_l = 1{,}75$, and 1,42 the pressure gradient is favorable to $x/c = 60$ per cent, and the transition occurs somewhat farther back, at $x/c = 72$ per cent. At $c_l = 1{,}14$ the pressure gradient is nearly zero over a large portion of the lower surface. This is the region where the large extent of unstable laminar boundary layer exists, as mentioned in the foregoing chapter. At $c_l = 0{,}92$, a minimum pressure peak forms at $x/c = 14$ per cent, nevertheless the boundary layer remains laminar back to $x/c = 68$ per cent. As the lift coefficient decreases, the pressure peak becomes more and more pronounced and the transition moves rapidly forward due to the severe adverse pressure gradient. That this pressure peak development contributes considerably to the profile drag at low lift coefficients will be pointed out in the consecutive chapters.

Momentum Thickness and Form Parameter of the Boundary Layer

The boundary layer profiles, examples of which were shown in Figures 4 and 5, were integrated to obtain the displacement and momentum thickness of the boundary layer which are defined as:

$$\delta^* = \int_0^\delta \left(1 - \frac{u}{U}\right) dy$$

and

$$\Theta = \int_0^\delta \frac{u}{U}\left(1 - \frac{u}{U}\right) dy$$

where δ is the thickness of the boundary layer, u/U the velocity ratio and y the coordinate normal to the surface. It was pointed out in Figure 6, that the character of the boundary layer development is opposite on the upper and lower surface. The upper surface provides a large extent of laminar boundary layer at $c_l < 0{,}8$, while the lower surface does that at $c_l > 0{,}8$. This contrasted behavior appears very distinctly in the growth of the momentum thickness along the chord which is illustrated in Figure 9. In the laminar boundary layer the growth is very slow and the absolute value of Θ ranges between 0,1 and 0,5 thousandths of the chord length. In the turbulent boundary layer the rate of the growth is considerably greater and varies according to the lift coefficient and chordwise position. Apparently the adverse pressure gradient against which the flow must travel has a great influence on the growth of the momentum thickness. The stronger the adverse gradient, the more rapid is the growth. The conditions are particularly severe on the upper surface at high lift coefficients, when a laminar separation bubble occurs near the leading edge and results in a rapidly growing turbulent boundary layer. An increased rate of growth is also apparent when laminar separation takes place at about $x/c = 75$ to 80 per cent on the upper surface at low lift coefficients.

Since the boundary layer measurements did not extend further back than $x/c = 85$ per cent on the upper surface and $x/c = 90$ per cent on the lower surface, the curves are extrapolated to the trailing edge. This, of course, implies some uncertainty in the calculation of the profile drag development discussed later. At the test station, $x/c = 10$ per cent, the boundary layer was so thin that the profiles recorded were not suitable for evaluation; therefore, the curves are shown only for $x/c = 20$ per cent.

The growth of the momentum thickness, except for the very high lift coefficients, is more intense on the lower surface. Particularly, at the low lift coefficients, a 4 to 6 times thicker boundary layer develops on the lower surface than on the upper surface. This calls attention to the thought that a considerable portion of the profile drag may be due to the lower surface which is usually considered of secondary importance.

Figure 10 illustrates the variation of the boundary layer form parameter, $H = \delta^*/\Theta$, along the chord for several lift coefficients. When the boundary layer is laminar, the form parameter ranges in value from $H = 2{,}0$ to 2,6. At the transition H suddenly falls to about 1,4, which corresponds to a stable turbulent boundary layer. After transition the form parameter remains nearly constant for a certain distance, then begins gradually to increase. When it reaches the critical limit of $H \cong 2{,}0$, the turbulent boundary layer separates.

In some cases, on the upper surface, the form parameter is of growing tendency due to the instability of the laminar

boundary layer. Laminar separation occurs when the critical limit of $H = 3{,}1 \sim 3{,}2$ is reached. In the separated laminar boundary layer the form parameter rises to a considerably higher value, however, this is somewhat of an arbitrary interpretation, because the theorems of the displacement and momentum thickness are valid only for separation-free flow.

Since the separated laminar boundary layer on the upper surface is assumed to re-attach as a turbulent one at about $x/c = 90$ per cent, the curves of the form parameter are extrapolated accordingly.

Profile Drag Analysis

The knowledge of the momentum thickness, form parameter, and velocity distribution around the airfoil enabled us to carry out an approximate calculation for the drag development on both the upper and lower surfaces. This was particularly aimed at delineating the contribution of each of the individual sides to the total profile drag. The following formula, given by Squire and Young [8], was used to calculate the drag:

$$c_{d_p} = \frac{\Theta}{c}\left(\frac{U}{V}\right)^{\frac{H+5}{2}}$$

In this formula, besides the friction which constitutes the major part, the pressure drag is included also. However, the formula was derived for separation free flow, consequently that part of the pressure drag which originates from separation is not included. Therefore, in the present case, since some sort of separation occurs throughout most of flight regime, we cannot expect a good agreement between the calculated and measured profile drag data. There is another difficulty which implies further uncertainty in the calculation, that is, that only extrapolated values of the boundary layer parameters are available for the trailing edge, where the boundary layer reaches its final, fully developed stage. In spite of these difficulties an estimation of the profile drag is thought to be useful in getting preliminary information as to how the profile drag is divided between the upper and lower surfaces.

Figure 11 shows the profile drag development along the airfoil for several lift coefficients. The curves generally have similar characteristics to those of the momentum thickness, shown in Figure 9. On the upper surface extremely high drag develops at high lift coefficients, due to the rapidly growing turbulent boundary layer and the high velocity ratio. The high drag is further increased by turbulent separation on the rear part of the airfoil. In order to illustrate this, the actual value of the upper surface drag[2] is also indicated for two cases, $c_l = 1{,}14$ and $c_l = 0{,}92$, and chain lines represent the sudden drag increase from the starting point of the turbulent separation.

How much drag increment can be attributed to the laminar separation occurring on the rear part of the airfoil at low lift coefficients has been an unanswered question. Our calculated data suggest that the drag is at least doubled; however, the reliability of the calculation for separated flow is doubtful.

A significant result of the calculation is that it points out that the drag contribution of the lower surface at low lift coefficients is about three times higher than that of the upper surface.

In Figure 12 the profile drag polar is broken down into its components. The sum of the upper and lower surface drag represents the calculated profile drag polar. The difference between this and the measured profile drag polar is considered as pressure drag due to separation. A compendium of the boundary layer development is given also in Figure 12. This shows that there is only a small range of lift coefficients between $C_L = 0{,}65$ and $0{,}85$, where the flow is completely free of separation. Interestingly, in this region there is quite good agreement between the measured and calculated data. This confirms that the difference can be attributed to separation. Thus, we have gained valuable information

[2] Measured profile drag minus calculated lower surface drag

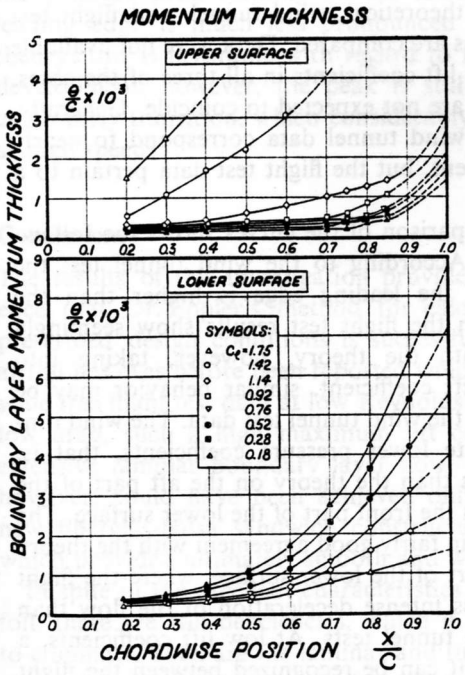

Fig. 9

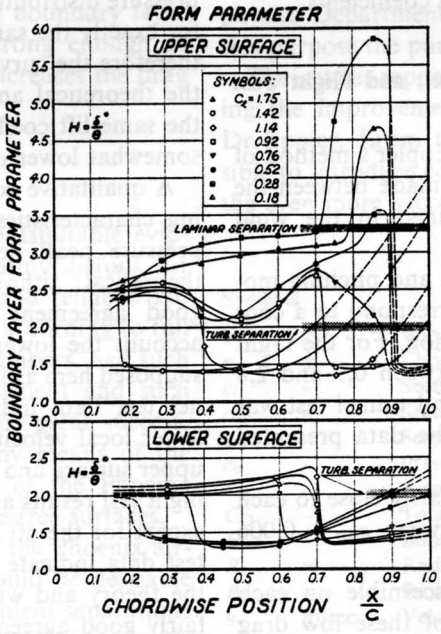

Fig. 10

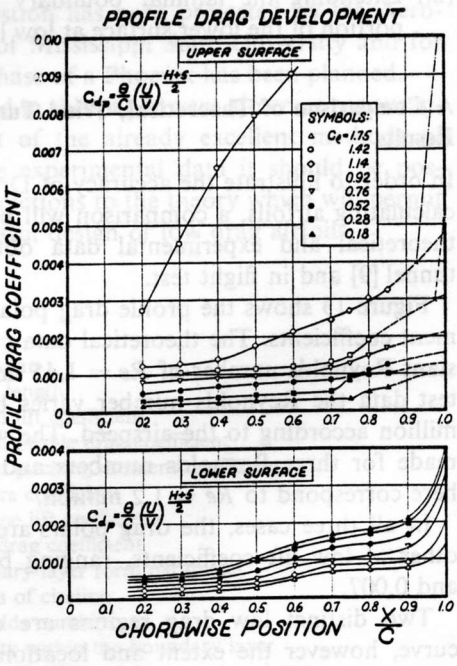

Fig. 11

about the order of magnitude of the separation drag, which is difficult to calculate.

Above $c_l = 0{,}85$, when turbulent separation takes place on the upper surface, the profile drag is nearly doubled. Below $c_l = 0{,}55$, both laminar separation on the upper surface and turbulent separation on the lower surface take place at the same time. Therefore, it is difficult to separate their effect. The turbulent separation on the bottom, however, is not severe and probably limited to a small area around

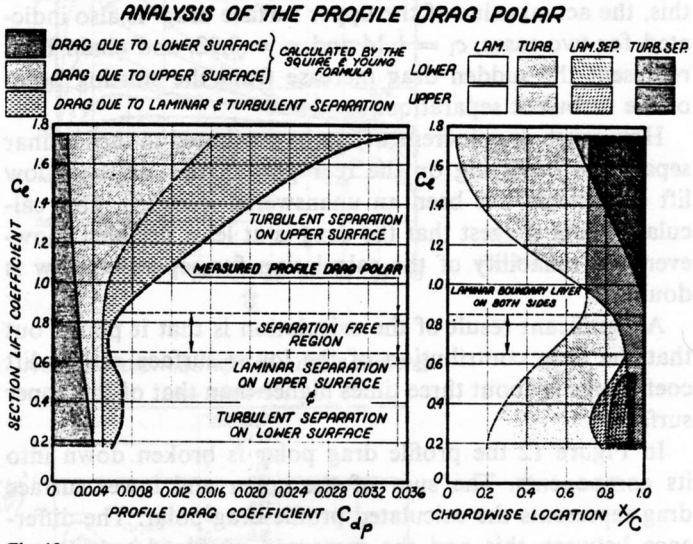

Fig. 12

ence is that the theoretical polar shows low drag up to $c_l = 1{,}05$, while the experimental curves indicate the beginning of severe drag increase, due to turbulent separation, at $c_l = 0{,}65$ in the case of the wind tunnel data and at $c_l = 0{,}80$ for the flight test data. The drag increase is most rapid in the case of the flight tested polar, however, the maximum lift coefficient, $c_{l\,max} = 1{,}75$ is much greater than the theoretical value and the wind tunnel result, which are $c_{l\,max} = 1{,}40$ and $c_{l\,max} = 1{,}45$, respectively.

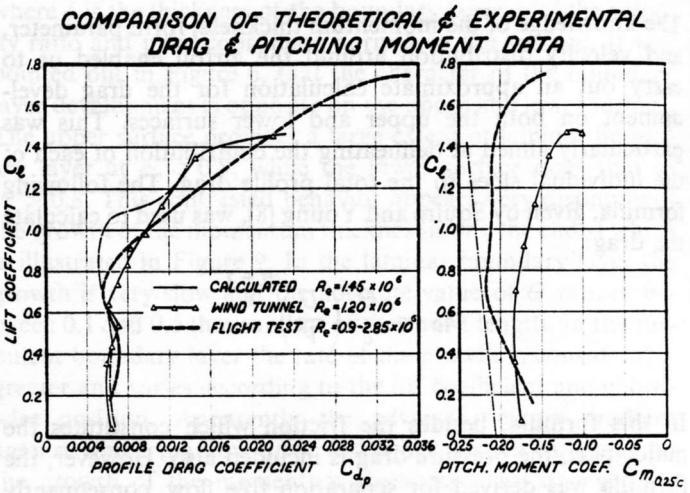

Fig. 13

$x/c = 85$ to 95 per cent. Consequently, it is suspected that the greater part of the separation drag is due to the laminar separation.

On the basis of the profile drag analysis it can be concluded that in spite of the excellent characteristics of the Phoenix airfoil, there is still great possibility of improvement. Further development should be directed toward:

(1.) Preventing laminar and turbulent separation on the upper surface, and,

(2.) Extending the laminar boundary layer over a larger portion of the lower surface at low lift coefficients.

A Comparison of Theoretical, Wind Tunnel, and Flight Test Results

In order to illustrate the accuracy of Dr. Eppler's method of calculating airfoils, a comparison will be made between the theoretical and experimental data obtained in the wind tunnel [9] and in flight test.

Figure 13 shows the profile drag polars and pitching moment coefficients. The theoretical data correspond to a constant Reynolds number of $Re = 1{,}45$ million. For the flight test data the Reynolds number varies between 0,9 and 2,8 million according to the airspeed. The wind tunnel test was made for three Reynolds numbers and the data presented here correspond to $Re = 1{,}2$ million.

In all three cases, the drag polars are fairly close to each other at low lift coefficients, ranging between $c_{dp} = 0{,}006$ and 0,007.

Two distinct low drag regions are discernible on each curve, however the extent and location of these low drag "buckets" are somewhat different. The most striking differ-

The theoretical pitching moment coefficient is linear over the entire c_l range with $c_{mo} = -0{,}205$. The flight test results calculated from the pressure distribution, show a nearly constant pitching moment of $c_{m \cdot 25c} = -0{,}21$ at lift coefficients between $c_l = 0{,}6$ and 1,4. Below and above these c_l values the pitching moment coefficient decreases to about $c_{m \cdot 25c} = -0{,}15$. According to the wind tunnel test, $c_{m \cdot 25c}$ has a nearly constant value of $c_{m \cdot 25c} \cong -0{,}18$ below $c_l = 0{,}8$, and it gradually decreases at the higher lift coefficients to $c_{m \cdot 25c} = -0{,}10$.

In Figure 14 the theoretical, wind tunnel, and flight test pressure distributions are compared. Data were not available for exactly the same lift coefficients in all three of the cases, therefore the curves are not expected to coincide. Generally, the theoretical and wind tunnel data correspond to nearly the same lift coefficient, but the flight test data pertain to a somewhat lower c_l.

A qualitative comparison of the curves shows the following characteristics: According to the wind tunnel test the pressure peak near the leading edge is higher than the theoretical; although the flight test results show seemingly good agreement with the theory, however, taking into account the lower lift coefficient, similar behavior may be supposed here as for the wind tunnel test data. The wind tunnel test data indicate lower pressure coefficients, that is, lower local velocities than the theory on the aft part of the upper surface and on the front part of the lower surface. The flight test results are in fairly good agreement with the theory except for the aft part of the lower surface, where the flight test data indicate less intense deceleration of the flow than the theory and wind tunnel tests. At low lift coefficients, a fairly good agreement can be recognized between the flight test and wind tunnel results, and significantly, in both cases

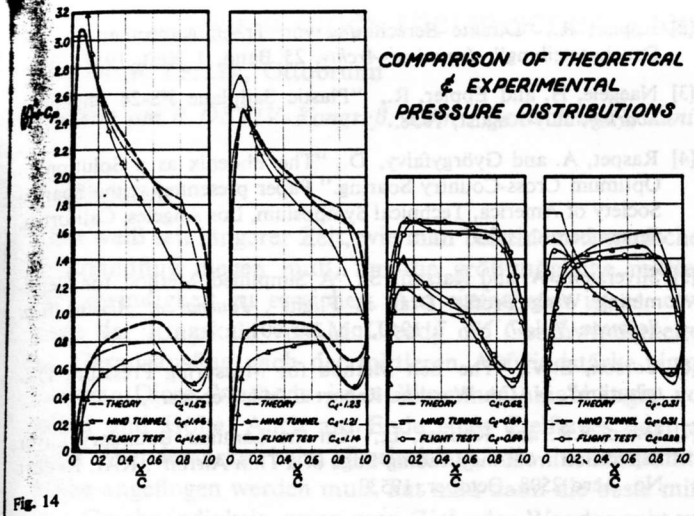

Fig. 14

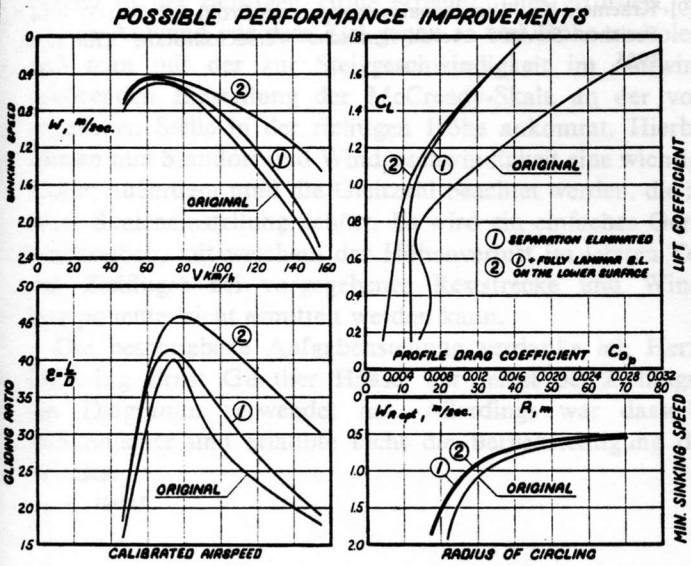

Fig. 15

the pressure peak forming on the lower surface near the leading edge is much less pronounced than predicted by theory; this is favorable with regard to the boundary layer development, however, the peak is still strong enough to cause early transition, which considerably increases the drag at high speeds.

Conclusions

The results of this investigation provide indisputable evidence that Dr. Eppler's method for calculating airfoils for prescribed design conditions is successful and reliable. No airfoil has ever before been reported which, according to full scale free flight test data at low Reynolds numbers, had such low drag, such a high maximum lift coefficient and such extensive laminar boundary layer flow. This great success, however, could have been achieved only by means of the new fiberglas-balsa sandwich construction of the Phoenix which provided ultimately smooth and wave-free surfaces.

In spite of the excellent characteristics of the Phoenix airfoil, there are still deficiencies, which it would be desirable to eliminate. Such are the laminar and turbulent separations on the upper surface as well as the early transition and rapidly growing turbulent boundary layer on the lower surface at low lift coefficients.

It is beyond the scope of this paper to discuss in detail the practical possibilities of improving the deficiencies, however, a brief perspective will be given to outline what improvements could be expected in the performance of the Phoenix by certain reductions in the profile drag. The various conditions are illustrated in Figure 15, where the performance curves are shown for three different profile drag polars: One represents the present state according to the flight test data, and the other two are derived from the following assumptions: That (1) teh laminar and turbulent separation are completely eliminated; (2) in addition to the above, the boundary layer is kept laminar along the entire lower surface. In the former case the profile drag polar is the same as calculated by the Squire and Young formula and shown in Figure 11. Here, $c_{dp} = 0{,}005$ for $C_L \leqq 0{,}9$ and the drag grows moderately above this lift coefficient. In the second case, with a fully laminar boundary layer on the lower surface, a very low minimum profile drag coefficient, $c_{dp\,min} = 0{,}002$, could be achieved. At the higher lift coefficients, however, the favorable effect of the laminarization of the lower surface gradually decreases and the polar curve tends toward that of the previous case. While the elimination of the separation would improve the flight performances mostly in low speed flight and would barely increase the maximum gliding ratio, the laminarization of the lower surface offers a much larger order of performance improvement. The best gliding ratio would rise to 46 and the high speed performance would be nearly doubled.

These improvements would be practically impossible to achieve at the present state of the art it seems by means of simple geometric modification of the airfoil contour or by additional smoothing of the surface. They seem feasible only by the application of suction boundary layer control. The power required for suction, of course, presents a great problem in motorless flight, but some means for this certainly could be developed in the future if the necessity of suction boundary layer control for very high performance sailplanes were proven.

A further experimental investigation concerning the improvements in question has been projected by the Aerophysics Department of Mississippi State University and for this purpose the purchase of a Phoenix has been planned.

The studies reported in this paper were aimed at encouraging the improvement of the already excellent methods of Dr. Eppler. From the experimental data it should be possible to introduce corrections to the theory which will permit the even more successful design of low drag airfoils.

Symbols

b	m	Wing span
c	m	Chord length
c_l	–	Section lift coefficient
c_{dp}	–	Section profile drag coefficient
c_m	–	Section pitching moment coefficient
c_p	–	Pressure coefficient
C_L	–	Airplane lift coefficient
C_D	–	Total drag coefficient
H	–	Boundary layer form parameter
R	m	Radius of circling
Re	–	Reynolds number
u	m/sec	Velocity within the boundary layer
U	m/sec	Velocity outside of the boundary layer

V	km/h	Calibrated airspeed
w	m/sec	Sinking speed
w_{Ropt}	m/sec	Minimum sinking speed in circling flight
x	m	Distance from leading edge along the chord
y	m	Distance perpendicular to the airfoil surface
δ	–	Induced drag increment
δ	m	Boundary layer thickness
δ^*	m	Boundary layer displacement thickness
Θ	m	Boundary layer momentum thickness
ε	–	Gliding ratio
λ	–	Aspect ratio

Acknowledgement

This research was supported by the United States Army Transportation Command and Office of Naval Research. The authors are indebted to Mr. L. Bölkow, Dr. R. Eppler, and Mr. H. Naegele for their cooperation that enabled this study to be undertaken. Also, the authors wish to express their appreciation to those members of the Aerophysics Department who participated in this project.

References

[1] Raspet, A., "Systematic Improvement of the Drag Polar of the Sailplane RJ-5", *Soaring*, 1951, No. 5.

[2] Eppler, R., "Direkte Berechnung von Tragflügelprofilen aus der Druckverteilung", *Ingenieur-Archiv*, 25. Band, 1. Heft, 1957.

[3] Naegele, H. and Eppler, R., "Plastic Sailplane FS-24 Phoenix", *Soaring*, July-August, 1958.

[4] Raspet, A. and Györgyfalvy, D., "The Phoenix as a Solution to Optimum Cross-Country Soaring." Paper presented at the Soaring Society of America, Technical Symposium, Los Angeles, California, September 12, 1959.

[5] Silverstein, A. and Katzoff, S., "A Simplified Method for Determining Wing Profile Drag in Flight", *Journal of Aeronautical Sciences*, Vol. 7, No. 7, 1940, pp. 295/301.

[6] Corson, B.W., "The Belt Method for Measuring Presssure Distribution", NACA Wartime Report L-244, February, 1943.

[7] Owen, P.R. and Klafner, L., "On the Laminar Boundary Layer Separation from the Leading Edge of a Thin Airfoil", RAE Report No. Aero 2508, October, 1953.

[8] Squire, H.B. and Young, A.D., "The Calculation of the Profile Drag of Airfoils", ARC Report No. 1838, 1938.

[9] Kraemer, K., "Windkanalmessungen am Profil EC 86 (-3) -914." Bericht: 56/A/05 Aerodynamische Versuchsanstalt, Göttingen, 1956.